RADC-TR-65-186, Vol. IV
Final Report

ANTENNA LOBE SUPPRESSION

Volume IV - The H-Plane Radiation Pattern of Horn Antennas

J. S. Yu
R. C. Rudduck

TECHNICAL REPORT NO. RADC-TR-65-186
October 1965

Vulnerability Reduction Branch
Rome Air Development Center
Research and Technology Division
Air Force Systems Command
Griffiss Air Force Base, New York

ANTENNA LOBE SUPPRESSION

Volume IV - The H-Plane Radiation Pattern of Horn Antennas

J. S. Yu
R. C. Rudduck

AFLC, AFB, N.Y.

ABSTRACT

Diffraction theory is used to formulate the H-plane radiation pattern of a horn antenna. Excellent agreement between computed and measured patterns is achieved by considering contributions from both the principal H-plane and E-edge diffractions.

The pattern is computed by superposition of various diffracted rays which are described by wedge diffraction as given in Appendix A. This technique is demonstrated to be accurate and practical without employing aperture integration techniques.

TABLE OF CONTENTS

THE H-PLANE RADIATION PATTERN OF HORN ANTENNAS

I. INTRODUCTION

The overall radiation pattern in the E-plane of a horn antenna has been successfully calculated[1] by using diffraction theory (in Appendix A) developed by Sommerfeld and Pauli. The techniques employed are successive evaluation of diffracted fields at various wedges and algebraic superposition of the various fields to form the total pattern. In this report the same techniques are employed to predict the radiation patterns in the H-plane of a horn antenna.

The excitation in the H-plane of the antennas must be treated differently from that in the E-plane; for the H-plane the primary source of radiation is the two plane waves (shown in Fig. 1) illuminating wedges A and B. The diffracted waves at A and B can be solved by Pauli's solutions. But interactions between the diffracted waves cannot be described accurately without including the higher-order terms of Eq. (A-3) given by Pauli in Appendix A. This limitation occurs for wide-angle wedges at A and B in which the distance between A and B is less than one wavelength. Instead of considering the higher-order terms in Pauli's solution, a new diffraction coefficient is developed at the end of Appendix A for this purpose.

In 1962, Kinber[2] used mode theory to solve the propagation modes inside the antenna horn and the solutions were used for illumination intensities in both E- and H-planes. In our present problem the solutions of mode theory are avoided by simply evaluating the diffracted waves at A and B. This makes possible a unique description of the problem by diffraction theory. In 1963, diffraction theory had been used by Peters and Rudduck[3] to study radiation mechanisms in the H-plane of a horn antenna. Experimentally they showed how the diffracted fields from E-edges (i.e., edges of the two horn walls which are perpendicular to the E-fields) can be eliminated from the principal H-plane pattern by applying RAM(Radar Absorber Materials) to the horn edges. Analytically, Ohba[4] used diffraction theory in the same year to compute the H-plane pattern of a corner reflector excited by a dipole source. No completely computed pattern is given, but excellent agreement is confirmed with measured patterns. It was pointed out that disagreement in the back-lobe region results from neglecting the diffracted fields from E-edges. In view of the

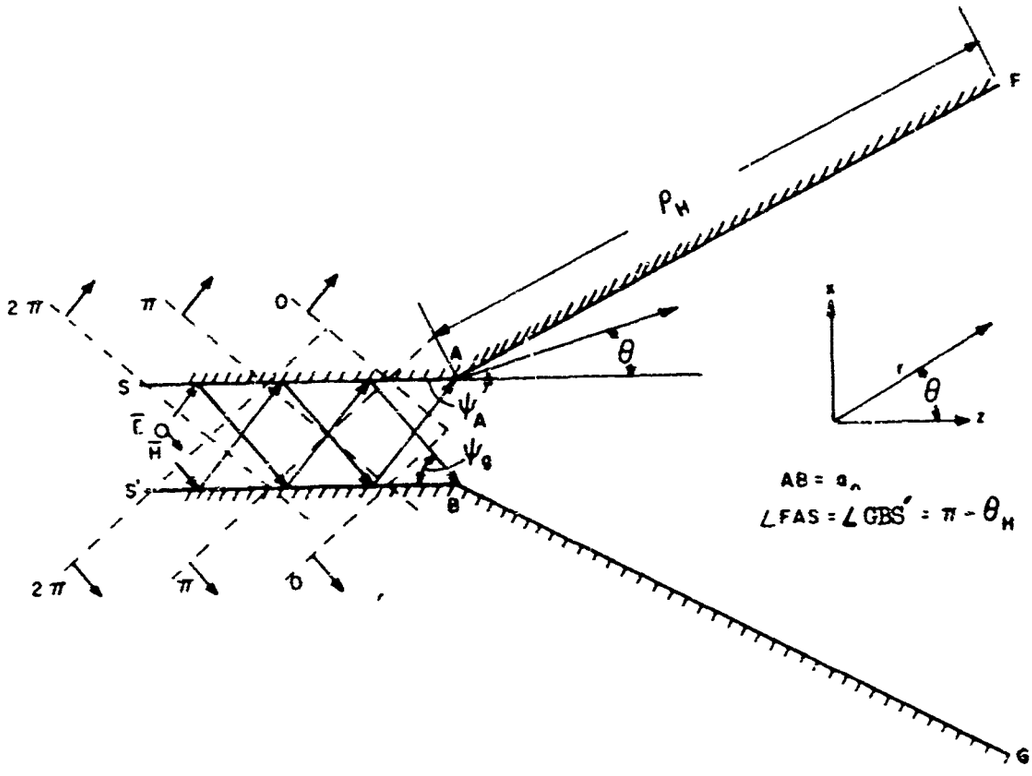

Fig. 1. Two component-plane-waves in the H-plane of a waveguide supporting TE_{10} mode.

significant contribution from the E-edge diffracted fields, we shall include this in the final H-plane patterns. To show the accuracy of predictions by diffraction theory, the problem will be formulated to compute a complete pattern which can be easily compared with experimental results.

II. RADIATION MECHANISMS

Propagation of electromagnetic waves inside a rectangular waveguide supporting the TE_{10} mode can be illustrated[5] by a simple physical picture of plane waves. The H-plane (i.e., the principal plane to which the H-field is parallel) of a horn antenna fed by the waveguide is shown in Fig. 1. The dotted lines represent three equiphase planes of the two

component-plane-waves. The arrowed solid lines represent the ray paths of the propagating TE_{10} mode. The purpose here is to investigate the radiation characteristics of the horn antenna excited by the guide at the throat AB.

The problem is a two-dimensional one in the principal H-plane of the antenna. The geometry shown in Fig. 1 is symmetrical with respect to $\theta = 0$, and this property of symmetry is used to simplify the following discussions. By the diffraction theory reviewed in Appendix A, two wedges, A and B, at the joint between the guide and the horn are said[6] to be illuminated by the incident plane waves. Cylindrical waves are diffracted from A and B; the diffracted rays from A are shown in Fig. 2. Each of the diffracted waves from A and B illuminates the opposite wedge and causes higher-order diffractions. This process of interaction between A and B continues indefinitely with successively decreasing illumination intensities, which are denoted coupling coefficients. The coupling coefficient between A and B can be formulated in closed form to obtain the resultant waves diffracted from A and B.

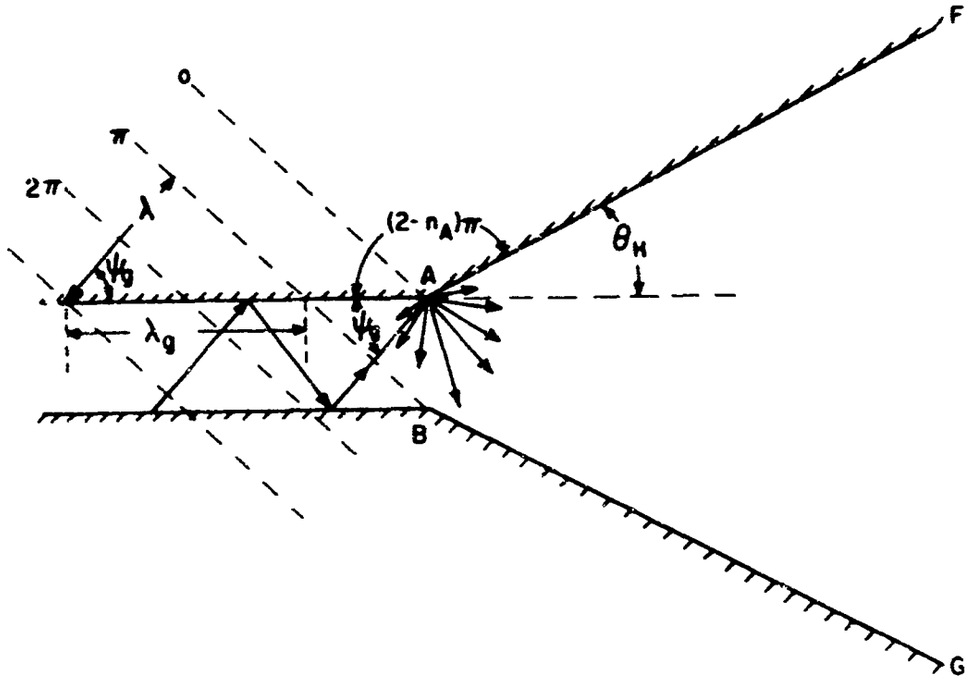

Fig. 2. Wedge A illuminated by one of the component-plane-waves in the guide.

The total diffracted waves may be divided into two portions. Consider wedge A in Fig. 3; the diffracted rays in the region $\angle SAB$ are reflected back into the guide while those in the region $\angle FAB$ propagate forward to the horn. The former portion is responsible for

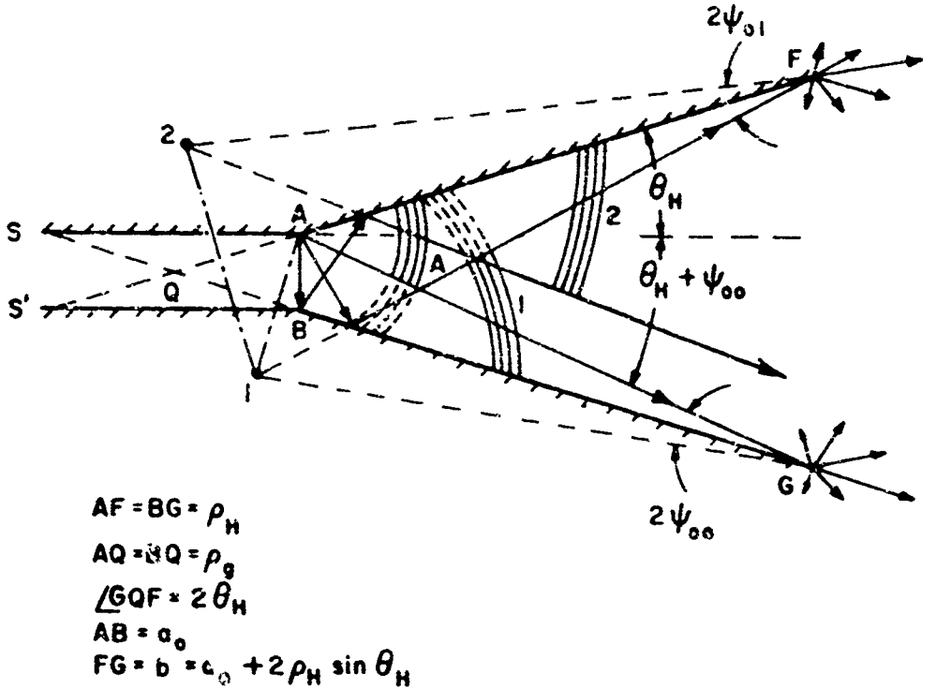

Fig. 3. The diffracted waves from wedge A and the two image-waves from Images 1 and 2.

mismatch between the guide and the horn. The latter portion may further be divided into several regions. In the region $\angle FAG$, four successive wavefronts are shown in solid curves to represent the portion of the wave which propagates directly to the far-field zone. The other portion (shown in dotted curves) is reflected by the wall BG. The reflected portion can be represented by the image formed by A. The image is shown at point 1; also only the portion shown in solid curves propagates to the far-field. The portion of the image-wave shown by dotted curves from point 1 is reflected by the wall AF, and a second image is formed at point 2. The last portion of the diffracted wave from A is now totally radiated to the far-field zone by the horn antenna. By the property of symmetry, two other symmetrical images can be constructed for the diffracted waves from wedge B. Consequently, four images formed by A and B can be constructed and all together six segments of cylindrical waves are

radiated from the interior of the antenna. Figure 4 shows the three segments from the lower half of the antenna. The discontinuities of the segmented cylindrical waves are all conpensated by introducing higher-order diffractions.

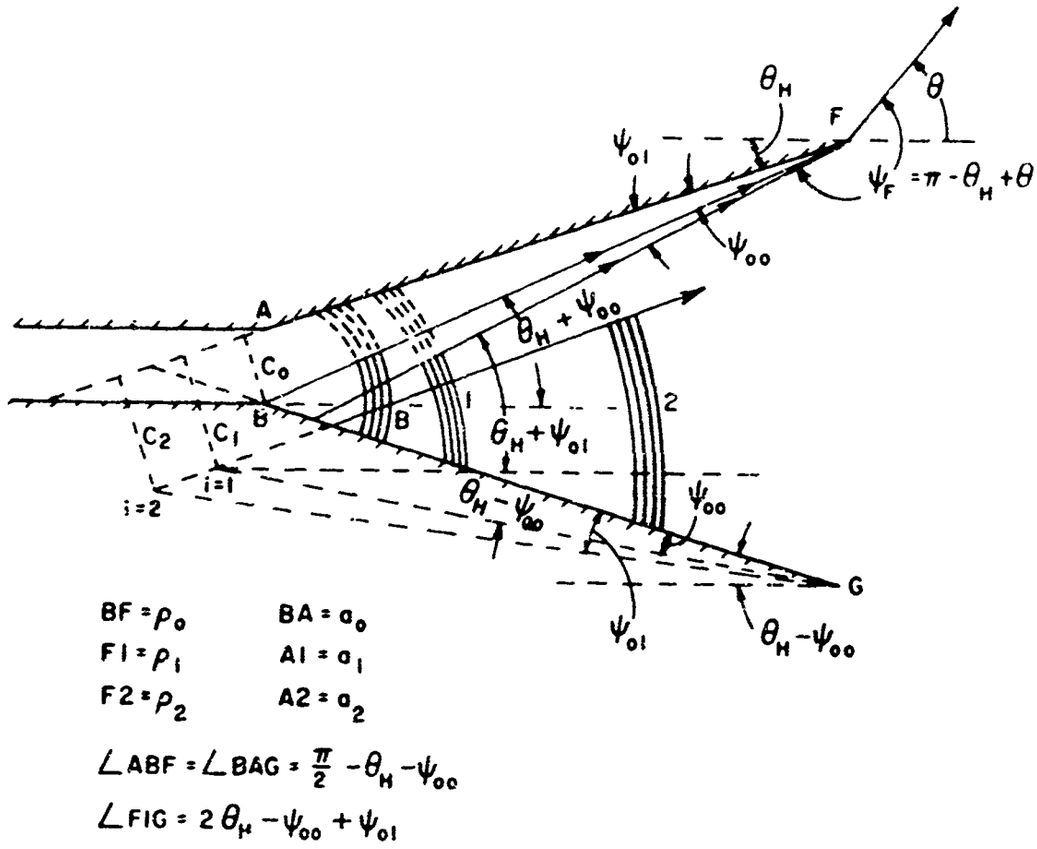

Fig. 4. Geometry of the lower-wall image-waves.

As the diffracted waves from A and B and their image-waves propagate outward, the wedges F and G are illuminated by these waves. As a consequence, more diffracted waves are induced at F and G which contribute to the total radiation pattern. In Fig. 3, F and G are shown illuminated by a ray from image 1 and A, respectively. If all possible illuminations are properly taken into account, the resultant diffraction at F and G can be formulated. The diffracted waves at F and G also illuminate each other and a closed-form interaction can be obtained. The images formed in the horn walls by F and G are formulated in Appendix B.

The mechanisms of radiation of the horn antenna have been expressed in terms of diffraction theory. The total radiation pattern is the superposition of the four diffracted waves from wedges A, B, F, and G and all the image-waves formed in the horn walls. It has been shown[3] that the diffracted fields from E-plane edges of the horn also contribute to the principal H-plane pattern. This contribution is also formulated in the following section.

III. FORMULATION OF SOLUTION

The two plane waves illuminating A and B in Fig. 1 are in phase and equal in magnitude. The distance between A and B is denoted a_o and the incident angle can be obtained from Fig. 2 as

$$(1) \qquad \psi_g = \cos^{-1}\frac{\lambda}{\lambda_g} = \sin^{-1}\left(\frac{\lambda}{2a_o}\right) .$$

The direction of field-point referred to wedge A is

$$(2) \qquad \psi_A = \pi + \theta .$$

The wedge angle $\pi - \theta_H$ shown in Fig. 2 is set equal to $(2-n_A)\pi$, resulting in the value of n_A given by

$$(3) \qquad n_A = 1 + \frac{\theta_H}{\pi} .$$

If the illuminating plane waves are assumed to have unit intensity, the solutions of diffracted waves from wedge A can be obtained from Eq. (A-4) as

$$(4) \qquad D_{Ag}(\theta) = K_{A1}\left[\left\{K_{A2} - \cos\left(\frac{\pi-\psi_g+\theta}{n_A}\right)\right\}^{-1} - \left\{K_{A2} - \cos\left(\frac{\pi+\psi_g+\theta}{n_A}\right)\right\}^{-1}\right] ,$$

$$K_{A1} = n_A^{-1} \sin\left(\frac{\pi}{n_A}\right) ,$$

and

$$K_{A2} = \cos\left(\frac{\pi}{n_A}\right) ,$$

where the cylindrical wave factor

$$(2\pi kR)^{-\frac{1}{2}} \text{Exp.} \left[-j \left(\frac{\pi}{4} + kR\right)\right]$$

to the far-field point is suppressed because only angular dependence is of interest. The angles used for the incident and reflected terms are obtained by

$$\phi^i = \psi_A - \psi_g = \pi + \theta - \psi_g$$

and

$$\phi^r = \psi_A + \psi_g = \pi + \theta + \psi_g ,$$

where the superscripts i and r replace the signs ($\mp$) in Appendix A to indicate that the ϕ's are for the incident and reflected terms. By the property of symmetry, the diffracted waves from wedge B can be obtained by replacing θ in Eq. (4) by $(-\theta)$ as

$$(5) \qquad D_{Bg}(\theta) = D_{Ag}(-\theta) = K_{A1} \left[\left\{K_{A2} - \cos\left(\frac{\pi - \psi_g - \theta}{n_A}\right)\right\}^{-1} - \left\{K_{A2} - \cos\frac{\pi + \psi_g - \theta}{n_A}\right\}^{-1}\right]$$

$n_B = n_A$,

$K_{B1} = K_{A1}$, and $K_{B2} = K_{A2}$.

Only portions of the two diffracted waves obtained in Eqs. (4) and (5) propagate directly to the far field. These portions are schematically shown as solid-curved wavefronts in Figs. 3 and 4; the portions of the waves reflected by horn walls are shown in dotted curves. Before discussing reflections of the waves, it is first convenient to treat interactions between A and B. At the boundary $\psi_A = \pi/2$ or $\theta = -\pi/2$, the diffracted wave from A illuminates B with an intensity $D_{Ag}(\theta = -\pi/2)$. Similarly, A is illuminated by B by $D_{Bg}(\theta = +\pi/2)$. Using Eqs. (4) and (5), the coupling coefficient between A and B is obtained as

$$(6) \qquad C'_{AB} = D_{Ag}\left(\theta = \frac{-\pi}{2}\right) = D_{Bg}\left(\theta = \frac{\pi}{2}\right)$$

$$= K_{A1}\left[\left\{K_{A2} - \cos\frac{1}{n_A}\left(\frac{\pi}{2} - \psi_g\right)\right\}^{-1} - \left\{K_{A2} - \cos\frac{1}{n_A}\left(\frac{\pi}{2} + \psi_g\right)\right\}^{-1}\right] .$$

Assuming that the diffractions from A and B are the same as those obtained by illuminating each other with uniform waves of intensity C'_{AB}, the diffracted waves consequently induced at A and B may be obtained from Eqs. (A-3) as

$$(7) \qquad D'_{AB}(\theta) = C'_{AB}\left[v_B\left(a_o, \frac{\pi}{2} + \theta, n_A\right) - v_B\left(a_o, \frac{3\pi}{2} + \theta, n_A\right)\right] ,$$

$$D'_{BA}(\theta) = D'_{AB}(-\theta) ,$$

and

$$\phi_{AB}^{i,r} = \psi_A \mp \frac{\pi}{2} = \begin{cases} \frac{\pi}{2} + \theta \\ \frac{3\pi}{2} + \theta . \end{cases}$$

In Eq. (7) the incident angle from B to A is equal to $\pi/2$, and again the property of symmetry is used. The solutions in Eqs. (7) are 2nd-order diffractions which produce 3rd-order diffractions at A and B. The 2nd-order coupling coefficient can be obtained as

$$(8)\qquad D'_{AB}\left(\theta=-\frac{\pi}{2}\right) = D'_{BA}\left(\upsilon=\frac{\pi}{2}\right)$$

$$= C'_{AB}\left[v_B(a_o, 0, n_A) - v_B(a_o, \pi, n_A)\right]$$

$$= C'_{BA}\, C_{ABA},$$

where the triple-subscript is used to indicate that wedge A is illuminated by B at which the diffracted waves are induced by C'_{BA} from A. If the process of interactions between A and B is indefinitely continued, the resultant coupling coefficient can be obtained in closed form as

$$(9)\qquad C_{AB} = C_{BA} = \frac{C'_{AB}}{1-C_{ABA}},$$

which is evaluated by using Eqs. (6) and (8). As a result, the total diffracted waves resulting from the interactions have the same form of solutions as in Eq. (7), with C'_{AB} replaced by C_{AB}.

Combination of the diffracted waves in Eqs. (4) and (5) and that caused by the interactions between A and B can finally be written as

$$(10)\qquad D_A(\theta) = D_{Ag} + D_{AB}$$

$$= K_{A1}\left[\left\{K_{A2} - \cos\frac{\pi-\psi_g+\upsilon}{n_A}\right\}^{-1} - \left\{K_{A2} - \cos\frac{\pi+\psi_g+\upsilon}{n_A}\right\}^{-1}\right]$$

$$+ C_{AB}\left[v_B\left(a_o, \frac{\pi}{2}+\theta, n_A\right) - v_B\left(a_o, \frac{3\pi}{2}+\theta, n_A\right)\right]$$

$$-(\theta_H + \psi_{oo}) \le \theta \le \theta_H$$

and

$$D_B(\theta) = D_A(-\theta), \qquad \theta_H + \psi_{oo} \ge \theta \ge -\theta_H,$$

where the regions are specified so that the portions of waves reflected by horn walls are excluded. The values of D_A and D_B are set to zero outside the specified regions. The incidence angle ψ_{oo}^B can be determined from Fig. 4 as

$$(11) \qquad \psi_{oo} = \sin^{-1} \frac{c_o}{\rho_o} ,$$

$$c_o = a_o \cos \theta_H ,$$

and

$$\rho_o = (a_o^2 + \rho_H^2 + 2a_o\rho_H \sin \theta_H)^{\frac{1}{2}} .$$

The two resultant diffracted waves from A and B have been summarized in Eqs. (10) in which the regions are specified for only those rays which propagate directly to the far field. Since the solutions are symmetrical with respect to $\theta = 0$, the portions of the waves in the regions $(-\pi/2 \leq \theta \leq -(\theta_H + \psi_{oo})$ for A and $\pi/2 \geq \theta \geq (\theta_H + \psi_{oo})$ for B) reflected by the horn walls can be described similar to the methods in Appendix B. Using the property of symmetry and referring to Fig. 4, the images formed in the lower wall BG can be described in general, as in Eq. (B-8), by replacing θ in D_A in Eqs. (10) by $-(2i\theta_H + \theta)$:

$$(12) \qquad I_{Li}(\theta) = (-1)^i \left[D_A(\theta = -2i\theta_H - \theta) \right]$$

$$i = 1, 2, 3, \text{------} ,$$

where the factors $(-1)^i$ are used for each image because the electric field polarization is perpendicular to the plane of study. The number of images formed is determined by the horn geometry. In Figs. 3 and 4, the cylindrical wavefronts are drawn in order to emphasize the dividing regions for the images. For a horn with small θ_H and long ρ_H, the total extent of the region for each image may generally be expressed as

$$(13) \qquad (\Delta\theta)_i = 2\theta_H - \psi_{o(i-1)} + \psi_{oi} , \qquad i = 1, 2, 3 \text{ ----} ,$$

where

(14) $$\left.\begin{aligned}\psi_{oi} &= \sin^{-1}\frac{c_i}{\rho_i}\\ c_i &= a_i\cos(i+1)\theta_H\end{aligned}\right\}, \qquad i = 0, 1, 2 \text{ --- } ;$$

$$a_i = a_{i-1}\cos\theta_H + a_o\cos i\theta_H , \quad i = 1, 2, 3, \text{ --- } ;$$

and

$$\rho_i = [a_i^2 + \rho_H^2 + 2a_i\rho_H\sin(i+1)\theta_H]^{\frac{1}{2}} , \quad i = 0, 1, 2, \text{ --- } .$$

The notations are indicated in Fig. 4 in which ψ_{oi} are the incident angles of edge F from various images. Since the waves from A and B are reflected by the horn walls only in the region, $\angle ABF = \angle BAG = \pi/2 - \theta_H - \psi_{oo}$ as shown in Fig. 4, the sum of image regions should not exceed this value. This criterion is used here to determine the number of images; i.e.,

$$[2\theta_H - \psi_{oo} + \psi_{o1}] + [2\theta_H - \psi_{o1} + \psi_{o2}] + \text{---} [2\theta_H - \psi_{o(i-1)} + \psi_{oi}] \leq \frac{\pi}{2} - \theta_H - \psi_{oo}$$

or

$$(2i+1)\theta_H + \psi_{oi} \leq \frac{\pi}{2} .$$

In other words, the number of images is equal to the integer h which satisfies the condition

(15) $$(2h+1)\theta_H + \psi_{oh} \leq \frac{\pi}{2} ,$$

where the values of the ψ_{oi} are computed by Eqs. (14). When a set of θ_H, a_o, and ρ_H is given, the number of images formed in each horn wall by A and B can be determined by Eq. (15). From this information, the image-waves from the horn walls can be written from Eqs. (10) and (12) as

(16) $$I_{Li}(\theta) = (-1)^i\left[K_{A1}\left\{\left(K_{A2} - \cos\frac{\pi - \psi_g - 2i\theta_H - \theta}{n_A}\right)^{-1} - \left(K_{A2} - \cos\frac{\pi + \psi_g - 2i\theta_H - \theta}{n_A}\right)^{-1}\right\}\right.$$

$$+ C_{AB}\left\{V_B\left(a_o, \frac{\pi}{2} - 2i\theta_H - \theta, n_A\right) - V_B\left(a_o, \frac{3\pi}{2} - 2i\theta_H - \theta, n_A\right)\right\}\Bigg] ,$$

$$\psi_{o(i-1)} - \theta_H \leq \theta \leq \psi_{oi} + \theta_H$$

and

$$I_{Ui}(\theta) = I_{Li}(-\theta) , \quad -(\psi_{o(i-1)} - \theta_H) \geq \theta \geq -(\psi_{oi} + \theta_H)$$

$$i = 1, 2, 3, \cdots h ,$$

where the property of symmetry is used to obtain the image waves from the upper wall. Each term of the image waves in Eqs. (16) is valid only in the properly defined region, otherwise it is identically zero. If

$$[(2h + 1)\theta_H + \psi_{oh}] < \frac{\pi}{2} ,$$

the regions of the last terms, i = h in Eq. (16), should be modified as

(17) $\psi_{o(h-1)} - \theta_H \leq \theta \leq \frac{\pi}{2} - \psi_{o(h-1)} - (2h-1)\theta_H$, from the lower-wall,

and

$$-(\psi_{o(h-1)} - \theta_H) \geq \theta \geq -\left[\frac{\pi}{2} - \psi_{o(h-1)} - (2h-1)\theta_H\right], \text{ from the upper-wall.}$$

Examples of Eqs. (16) and (17) for h=2 may be obtained from Fig. 4.

We have so far described the diffracted waves from A and B, both directly to the far field by Eqs. (10) and indirectly reflected to the far field by Eqs. (16) and (17). When these waves propagate outward, wedges F and G are illuminated and diffracted waves are induced to contribute to the far field. Using Fig. 4 as an example, wedge F is illuminated by B and image 1 but not by image 2. In general, if there are h images formed in the lower wall, wedge F would be illuminated by B and (h-1) images in the directions $\theta = \theta_H + \psi_{oo}$ and $\theta = \theta_H + \psi_{oi}$, with i=1,2 ---(h-1). If the equality in Eq. (15) holds, then F would also be illuminated by the h^{th} image in the direction $\theta = \theta_H + \psi_{oh}$ but the intensity is equal to zero. To evaluate coupling coefficients in the mentioned directions, Eqs. (10) can first be used to obtain

$$C_{FB} = D_B(\theta = \theta_H + \psi_{oo})$$

$$= K_{A1}\left[\left\{K_{A2}-\cos\left(\frac{\pi-\psi_{oo}-\psi_g-\theta_H}{n_A}\right)\right\}^{-1}\right.$$

$$\left. - \left\{K_{A2}-\cos\left(\frac{\pi-\psi_{oo}+\psi_g-\theta_H}{n_A}\right)\right\}^{-1}\right]$$

$$+ C_{AB}\left[v_B\left(a_o, \frac{\pi}{2}-\psi_{oo}-\theta_H, n_A\right) - v_B\left(a_o, \frac{3\pi}{2}-\psi_{oo}-\theta_H, n_A\right)\right],$$

which can be seen to be identical to C_{Fi} shown below with i = 0. Therefore, coupling coefficients to F can be written from Eq. (16) in general as

(18) $$C_{Fi} = I_{Li}(\theta = \theta_H + \psi_{oi})$$

$$= (-1)^i\left[K_{A1}\left\{\left(K_{A2} - \cos\frac{\pi-\psi_g-\psi_{oi}-(2i+1)\theta_H}{n_A}\right)^{-1}\right.\right.$$

$$\left.\left. -\left(K_{A2}-\cos\frac{\pi+\psi_g-\psi_{oi}-(2i+1)\theta_H}{n_A}\right)^{-1}\right\}\right.$$

$$\left. + C_{AB}\left\{v_B\left(a_o, \frac{\pi}{2}-\psi_{oi}-(2i+1)\theta_H, n_A\right) - v_B\left(a_o, \frac{3\pi}{2}-\psi_{oi}-(2i+1)\theta_H, n_a\right)\right\}\right],$$

$$i = 0, 1, 2, ----(h-1),$$

where i=0 is included for $C_{FB} = C_{F0}$. By symmetry, the coupling coefficients from the upper wall to wedge G are $C_{Gi} = I_{Li}(\theta=-\theta_H-\psi_{oi})$, which are identical to C_{Fi} in Eqs. (18). With these coupling coefficients, the solutions of diffracted waves from F and G can be summarized by using Eqs. (A-3);

(19) $$D'_F = \sum_{i=0}^{h-1} C_{Fi}[v_B(\rho_i, \pi-\theta_H-\psi_{oi}+\theta, 2) - v_B(\rho_i, \pi-\theta_H+\psi_{oi}+\theta, 2)],$$

$$D'_G = D'_F(-\theta),$$

$$\phi^i_{Fi} = \psi_F - \psi_{oi} = (\pi - \theta_H + \theta) - \psi_{oi},$$

and

$$\phi^r_{Fi} = \psi_F + \psi_{oi} = (\pi - \theta_H + \theta) + \psi_{oi},$$

where i = (h-1) is set as the last term because the case for i = h has $C_{Gh} = 0$. Each of the diffracted waves D'_F and D'_G from F and G illuminates the opposite edge, causing a series of interactions, as is the case between A and B. In a manner similar to Eq. (9), the resultant coupling coefficient between F and G can be obtained as follows:

(20) $$C_{FG} = C_{GF} = \frac{C'_{FG}}{1-C_{FGF}},$$

$$C'_{FG} = D'_F\left(\theta = -\frac{\pi}{2}\right) = D'_G\left(\theta = \frac{\pi}{2}\right)$$

$$= \sum_{i=0}^{h-1} C_{Fi}\left[v_B\left(\rho_i, \frac{\pi}{2}-\theta_H-\psi_{oi}, 2\right) - v_B\left(\rho_i, \frac{\pi}{2}-\theta_H+\psi_{oi}, 2\right)\right],$$

and

$$C_{FGF} = v_B(b, 0, 2) - v_B(b, \pi - 2\theta_H, 2),$$

where C_{FGF} is the diffraction coefficient between F and G. Using C_{FG}, the diffracted waves from F and G resulting from the interactions can again be obtained by using Eq. (A-3) as

(21) $$D_{FG} = C_{FG}\left[v_B\left(b, \frac{\pi}{2}+\theta, 2\right) - v_B\left(b, \frac{3\pi}{2} - 2\theta_H + \theta, 2\right)\right],$$

$$D_{GF} = D_F(-\theta),$$

(21) (cont)
$$\psi^{i}_{FG} = \psi_F - \left(\frac{\pi}{2} - \theta_H\right) = \frac{\pi}{2} + \theta,$$

and

$$\psi^{r}_{FG} = \psi_F + \left(\frac{\pi}{2} - \theta_H\right) = \frac{3\pi}{2} - 2\theta_H + \theta,$$

where $\psi^{i,r}_{FG}$ are obtained from Fig. 4. The total diffractions from F and G are then the superposition of Eqs. (19) and (21) as

(22)
$$D_F = D'_F + D_{FG}$$

$$= \sum_{i=0}^{h-1} C_{Fi}\left[v_B(\rho_i, \pi-\theta_H-\psi_{oi}+\theta, 2) - v_B(\rho_i, \pi-\theta_H+\psi_{oi}+\theta, 2)\right]$$

$$+ C_{FG}\left[v_B\left(b, \frac{\pi}{2}+\theta, 2\right) - v_B\left(b, \frac{3\pi}{2}-2\theta_H+\theta, 2\right)\right],$$

$$-\frac{\pi}{2} \leq \theta \leq \pi + \theta_H;$$

and

$$D_G = D_F(-\theta), \qquad \frac{\pi}{2} \geq \theta \geq -(\pi+\theta_H),$$

where the regions are specified to exclude the portions of waves reflected by horn walls in the regions

$$-(\pi - \theta_H) < \theta < -\frac{\pi}{2} \text{ for F and } (\pi-\theta_H) > \theta > \frac{\pi}{2} \text{ for G.}$$

The portions of the diffracted waves from F and G which are reflected by the horn walls may be described in a manner identical to the image-waves in Appendix B. By Eq. (B-8), the image-waves in the lower and upper horn walls caused by F and G can be obtained from Eqs. (22) as

(23) $$I_{Lm}(\theta) = (-1)^m D_F(\theta = -2m\theta_H - \theta)$$

$$= (-1)^{in}\left[\sum_{i=0}^{h-1} C_{Fi}\{v_B(\rho_i, \pi - \psi_{oi} - (2m+1)\theta_H - \theta, 2)\right.$$

$$\left. - v_B(\rho_i, \pi + \psi_{oi} - (2m+1)\theta_H - \theta, 2)\}\right.$$

$$\left. + C_{FG}\left\{v_B\left(b, \frac{\pi}{2} - 2m\theta_H - \theta, 2\right) - v_B\left(b, \frac{3\pi}{2} - 2(m+1)\theta_H - \theta, 2\right)\right\}\right],$$

$$\frac{\pi}{2} - (m+1)\theta_H \leq \theta \leq \frac{\pi}{2} - m\theta_H ,$$

$$I_{Um}(\theta) = I_{Lm}(-\theta), \qquad -\left[\frac{\pi}{2} - (m+1)\theta_H\right] \geq \theta \geq -\left[\frac{\pi}{2} - m\theta_H\right] ;$$

and

$$m = 1, 2, 3\text{----}(p-1) ,$$

where p is the number of images formed in the lower or the upper wall, provided the walls FB and GA extend to intersect at Q. The value of p is the largest integer satisfying the condition

$$p < \frac{\pi}{2\theta_H} .$$

If the ratio $\pi/2\theta_H$ is not an exact integer, the region defined for the last image, i = p, should be modified as

(24) $$\frac{\pi}{2} - (m+1)\theta_H \leq \theta \leq \pi - (2m+1)\theta_H, \quad \text{from the lower-wall,}$$

and

$$-\left[\frac{\pi}{2} - (m+1)\theta_H\right] \geq \theta \geq -[\pi - (2m+1)\theta_H], \quad \text{from the upper-wall,}$$

in which most of the rays propagate into the guide as in Fig. 5. The image-waves given in Eqs. (23), in general, contribute negligibly to the total far-field pattern of typical horn antennas. But the contribution for

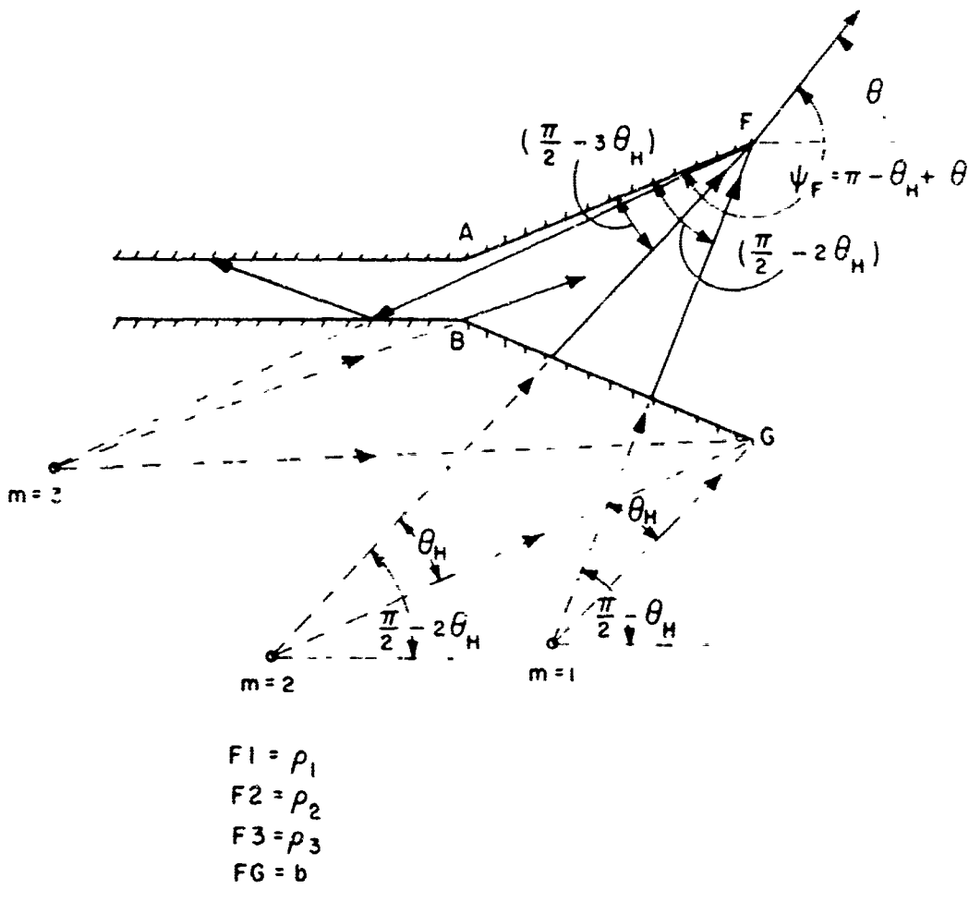

Fig. 5. The lower-wall images due to diffracted waves from wedges A and B.

small horns is not negligible. For very accurate treatment, the effects of Eqs. (23) may be included, and consequently their illuminations to wedges F and G need to be considered to compensate for discontinuities in Eqs. (23).

From the image regions given in Appendix B or Fig. 5, it can be seen that wedges F and G are illuminated by the lower and upper walls at

$$\theta = \pm \left(\frac{\pi}{2} - m\theta_H\right),$$

respectively, for each image. By using Eqs. (23) the coupling coefficients can be obtained as

$$(25)\qquad C_{Fm} = I_{Lm}\left(\theta = \frac{\pi}{2} - m\theta_H\right) = I_{Um}\left(\theta = -\frac{\pi}{2} + m\theta_H\right)$$

$$= (-1)^m \left[\sum_{i=0}^{h=1} C_{Fi}\left\{v_B\left(\rho_i, \frac{\pi}{2} - \psi_{oi} - (m+1)\theta_H, 2\right)\right.\right.$$

$$\left. - v_B\left(\rho_i, \frac{\pi}{2} + \psi_{oi} - (m+1)\theta_H, 2\right)\right\}$$

$$\left. + C_{FG}\{v_B(b, -m\theta_H, 2) - v_B(b, \pi - (m+2)\theta_H, 2)\}\right]$$

$$= C_{Gm}$$

$$m = 1, 2, 3\text{-----}(p-1)\ .$$

The value of m is restricted to (p-1) as the highest because the last image wave i=p does not exist for most horn antennas. The apparent reason is shown in Fig. 5 in which the diffracted rays giving rise to the last image actually propagate into the waveguide. In fact, for the small horn shown, a portion of the second to the last image does not exist either. Because of the fact that the diffracted-field intensity is very small for low angles of incidence, the contributions of I_{Lm}, I_{Um}, and C_{Fm} for the highest values of m are relatively insignificant. Therefore, a very satisfactory result can usually be obtained by considering the contributions only for m = 1 to (p-1).

Using C_{Fm} in Eqs. (25), the diffracted waves from F and G illuminated by the image-waves can be obtained as

$$(26)\qquad D_{Fm}(\theta) = C_{Fm}\left[v_B\left(\rho_m, \frac{\pi}{2} + m\theta_H + \theta, 2\right) - v_B\left(\rho_m, \frac{3\pi}{2} - (m+2)\theta_H + \theta, 2\right)\right]\ ,$$

$$D_{Gm}(\theta) = D_{Fm}(-\theta)\ ,$$

$$\rho_m = \rho_{(m-1)} \cos\theta + b \cos m\theta_H\ ,$$

$$\rho_o = b,$$

(26) (cont)
$$\theta^{i}_{Fm} = \psi_F - \left(\frac{\pi}{2} - (m+1)\theta_H\right) = \frac{\pi}{2} + m\theta_H + \theta,$$

and

$$\theta^{r}_{FM} = \psi_F + \left(\frac{\pi}{2} - (m+1)\theta_H\right) = \frac{3\pi}{2} - (m+2)\theta_H + \theta,$$

$$m = 1, 2, 3 \cdots (p-1),$$

where Fig. 5 can be used as reference for the geometry.

The total diffracted waves from F and G are then the sums of $D_F(\theta)$ and $D_G(\theta)$ in Eqs. (22) and $D_{Fm}(\theta)$ and $D_{Gm}(\theta)$ in Eqs. (26). Using subscript T to denote the total, they are obtained as

(27)
$$(D_F(\theta))_T = D_F + \sum_{m=1}^{p-1} D_{Fm}$$

$$= \sum_{i=0}^{h-1} C_{Fi}\left[v_B(\rho_i, \pi - \theta_H - \psi_{oi} + \theta, 2) - v_B(\rho_i, \pi - \theta_H + \psi_{oi} + \theta, 2)\right]$$

$$+ C_{FG}\left[v_B\left(b, \frac{\pi}{2} + \theta, 2\right) - v_B\left(b, \frac{3\pi}{2} - 2\theta_H + \theta, 2\right)\right]$$

$$+ \sum_{m=1}^{p-1} C_{Fm}\left[v_B\left(\rho_m, \frac{\pi}{2} + m\theta_H + \theta, 2\right) - v_B\left(\rho_m, \frac{3\pi}{2} - (m+2)\theta_H + \theta, 2\right)\right],$$

$$-\frac{\pi}{2} \leq \theta \leq \pi + \theta_H,$$

$$(D_G(\theta))_T = (D_F(-\theta))_T, \qquad \frac{\pi}{2} \geq \theta \geq -(\pi + \theta_H),$$

where C_{Fi}, C_{FG}, and C_{Fm} are given in Eqs. (18), (20) and (25), respectively.

For typical horn antennas, the diffraction process mentioned above is sufficient to describe the far-field radiation mechanisms. To obtain the total radiation pattern of the horn antenna one may simply superimpose the diffracted waves in Eqs. (10) and (27) and the corresponding images in Eqs. (16) and (23). It is noted that the images of D_{Fm} and D_{Gm} in Eqs. (26) are not included in Eqs. (23).

Before superimposing these waves to obtain the far-field pattern, a phase reference needs to be established. If F is taken as the phase-reference point, then phase-shift factors from A, B, G, and the images are given by

(28) $$y_{FA} = \text{Exp.}\left[+j2\pi\rho_H \cos\phi^i_{FA}\right];$$

$$y_{FB} = \text{Exp.}\left[+j2\pi\rho_o \cos\phi^i_{Fo}\right] = y_{Fi}\Big|_{i=0};$$

$$y_{FG} = \text{Exp.}\left[+j2\pi b \cos\phi^i_{FG}\right];$$

$$y_{Fi} = \text{Exp.}\left[+j2\pi\rho_i \cos\phi^i_{Fi}\right], \quad i = 1, 2\text{---- } h;$$

$$y_{Fm} = \text{Exp.}\left[+j2\pi\rho_m \cos\phi^i_{Fm}\right], \quad m = 1, 2, \text{--- } (p-1);$$

$$y_{Gi} = y_{Fi}(-\theta), \quad y_{Gm} = y_{Fm}(-\theta);$$

$$\phi^i_{FA} = \psi_A - \theta_H = \pi - \theta_H + \theta;$$

$$\phi^i_{FG} = \psi_A - \left(\frac{\pi}{2} - \theta_H\right) = \frac{\pi}{2} + \theta;$$

$$\phi^i_{Fi} = \psi_A - \psi_{oi} = (\pi - \theta_H + \theta) - \psi_{oi}, \quad i = 0, 1, 2 \text{ --- } h;$$

and

$$\phi^i_{Fm} = \psi_A - \psi_{om} = (\pi - \theta_H + \theta) - \left(\frac{\pi}{2} - (m+1)\theta_H\right)$$

$$= \frac{\pi}{2} + m\theta_H + \theta, \quad m = 1, 2 \text{ --- } (p-1),$$

where the distances ρ_H, b, ρ_i, and ρ_m are all in terms of wavelengths. The values of ψ_{oi} are given in Eqs. (14).

Finally, the radiation pattern of the horn antenna can be obtained by using Eqs. (10), (16), (23), (27), and (28) as

$$(29) \qquad u_H(\theta) = D_A y_{FA} + D_B y_{FB} + (D_F)_T + (D_G)_T y_{FG} + \sum_{i=1}^{h} [I_{Li}\, y_{Fi} + I_{Ui}\, y_{FG} y_{Gi}] + \sum_{m=1}^{p-1} [I_{Lm}\, y_{Fm} + I_{Um}\, y_{FG}\, y_{Gm}] , \qquad 0 \leq \theta \leq 2\pi ,$$

where each individual term is valid only in the properly defined region and otherwise is set to zero. The phase factors y_{Gi} and y_{Gm} are those of the image waves from the upper wall referred to G. When they are multiplied by y_{FG}, the phase reference of the upper wall images is referred to F.

It has been shown[3] that the radiation pattern in the H-plane of a horn antenna is not only due to contributions of H-plane radiation mechanisms, but also to diffracted fields from E-edges. It is assumed that the horn antenna shown in Fig. 6 has a geometrical-optics field distribution in the aperture which is constant in the E-plane and cosinusoidal from the center to the edges in the H-plane. Taking the upper horn wall for illustration, a ray initiated from an assumed source in the waveguide strikes the E-edge with an incident angle β shown. The incident ray-intensity is cosinusoidal from the center along the edge, therefore, if the intensity is assumed to be unity when $\beta = \pi/2$, the illumination intensity of the incident ray as a function of θ can be written as

$$(30) \qquad X(\theta) = \cos\left[\frac{\pi}{2} \tan\theta \cot\theta_H\right] , \qquad -\theta_H \leq \theta \leq \theta_H ,$$

where θ is in the H-plane. The diffracted rays from the edge form a cone and have a solution involving $\sin\beta$ [7] as

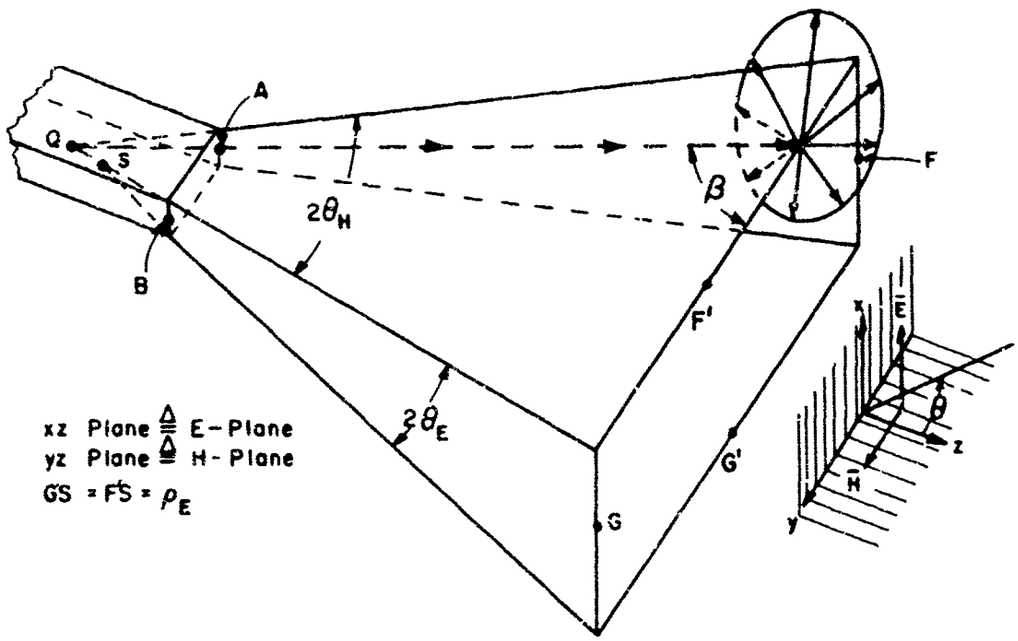

(a)

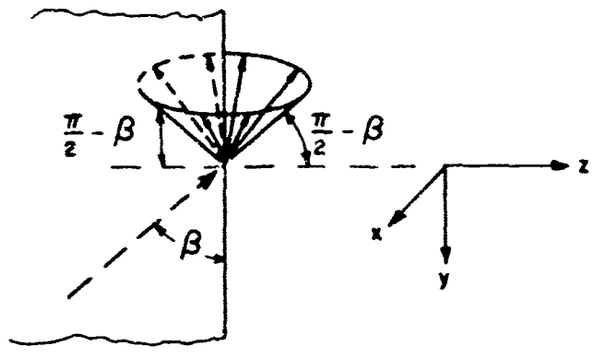

(b)

Fig. 6. Diffracted fields from E-plane.

$$(31) \qquad D = X(\theta)\,\frac{v_B(\rho_E, \pi - \alpha_E + \alpha, 2)}{\sin\beta},$$

where the angle α is referred to the principal E-plane of the antennas. The angle β in terms of θ is

$$(32) \qquad \beta = \frac{\pi}{2} - \theta.$$

Because only two of the diffracted rays shown in Fig. 6 lie in the H-plane, the v_B factors of Eq. (31) are given by

$$(33) \qquad v_B(\rho_E \sec\theta,\ \pi - \alpha_E, 2), \quad \text{in the forward direction,}$$

and

$$v_B(\rho_E\,|\sec\theta|,\ 2\pi - \alpha_E, 2), \quad \text{in the backward direction,}$$

where ρ_E is the horn length in the principal E-plane. Combining Eqs. (30) to (33), the diffracted fields contribution to the H-plane in the forward and backward directions are written as

$$(34) \qquad D_1 = \frac{\cos\left[\frac{\pi}{2}\tan\theta\cot\theta_H\right]}{\cos\theta}\,[v_B(\rho_E \sec\theta, \pi - \alpha_E, 2)], \quad -\theta_H \leq \theta \leq \theta_H,$$

and

$$D_2 = \frac{\cos\left[\frac{\pi}{2}\tan\theta\cot\theta_H\right]}{-|\cos\theta|}\,[v_B(\rho_E\,|\sec\theta|, 2\pi - \alpha_E, 2)], \quad \pi - \theta_H \leq \theta \leq \pi + \theta_H,$$

where the minus sign is introduced for D_2 to take into account the three-dimensional polarization properties of the contributions from the E-edges. Also taking into account the diffracted fields from the lower edge of the horn, the total contribution to the principal H-plane can be written as

$$(35) \qquad U_E(\theta) = 2u^*(0) \begin{cases} D_1 Y_{FD_1}, & -\theta_H \leq \theta \leq \theta_H \\ D_2 Y_{FD_2}, & \pi - \theta_H \leq \theta \leq \pi + \theta_H \end{cases},$$

where the factor $u^*(0)$ is the actual geometrical-optics field intensity instead of the unit intensity assumed earlier in Eq. (30). The value of

$u^*(0)$ can be obtained, within the accuracy of the solution in Eq. (29), in the direction of $\theta = 0$ as

$$(36) \qquad u^*(0) = 2 \left[D_A(0)\, y_{FA}(0) + \sum_{i=1}^{h} I_{Li}(0)\, y_{Fi}(0) \right] y_{SF}$$

and

$$y_{SF} = \text{Exp.}\,[j2\pi \rho_{SF} \cos \theta_H],$$

where the factor 2 results from contributions from both walls. The sum of the terms in the bracket has the phase-reference at edge F. The factor y_{SF} is used to refer $u^*(0)$ back to the assumed sourse S (the intersection of the two Walls perpendicular to E-fields) shown in Fig. 6, so that Eq. (35) is appropriate. The two phase factors in Eq. (35) are used to refer the diffracted rays to point F. They can be obtained by assuming, for convenience of computation, that $FS \approx FQ$ for typical horns. Under this assumption and making use of Figs. 4 and 6, the phase-factors can be obtained as

$$(37) \quad \left.\begin{matrix} y_{FD_1} \\ y_{FD_2} \end{matrix}\right\} = \text{Exp.}\left[-j2\pi \left\{ \frac{b}{2} - (\rho_H + \rho_g) \cos \theta_H \tan\theta \right\} \sin\theta \right], \quad \begin{cases} -\theta_H \leq \theta \leq \theta_H \\ \pi - \theta_H \leq \theta \leq \pi + \theta_H \end{cases}$$

where

$$\rho_g = \frac{a_o}{2 \sin \theta_H} \quad .$$

If the contributions from the E-edges given in Eq. (35) are considered in the H-plane radiation pattern given in Eq. (29), the total radiation pattern in the principal H-plane may now be written as

$$(38) \qquad u_T(\theta) = u_H(\theta) + U_E(\theta) \ .$$

To compute the radiation pattern , only the upper half-plane ($0 \leq \theta \leq \pi$) needs to be considered. Numerical computations will be discussed in the next section and compared with experimental results.

IV. COMPUTED RESULTS COMPARED WITH MEASURED PATTERNS

The horn antenna used in the experimental measurements is shown in Fig. 7a, in which the waveguide feeding the horn is finite in length and to which is attached an attenuator and a detector. It can be observed from the figure that any possible reflection and diffraction taking place on the surface of the guide and associated structure are not considered in the solutions given in Eqs. (29) and (35) or Eq. (38). Since the guide is finite in length and the diffracted waves from F and G illuminate A and B with zero intensity, the solutions in Eq. (38) can be applied to the approximate model shown in Fig. 7b. In other words, as far as H-plane-diffracted fields are concerned, the total pattern contributed by

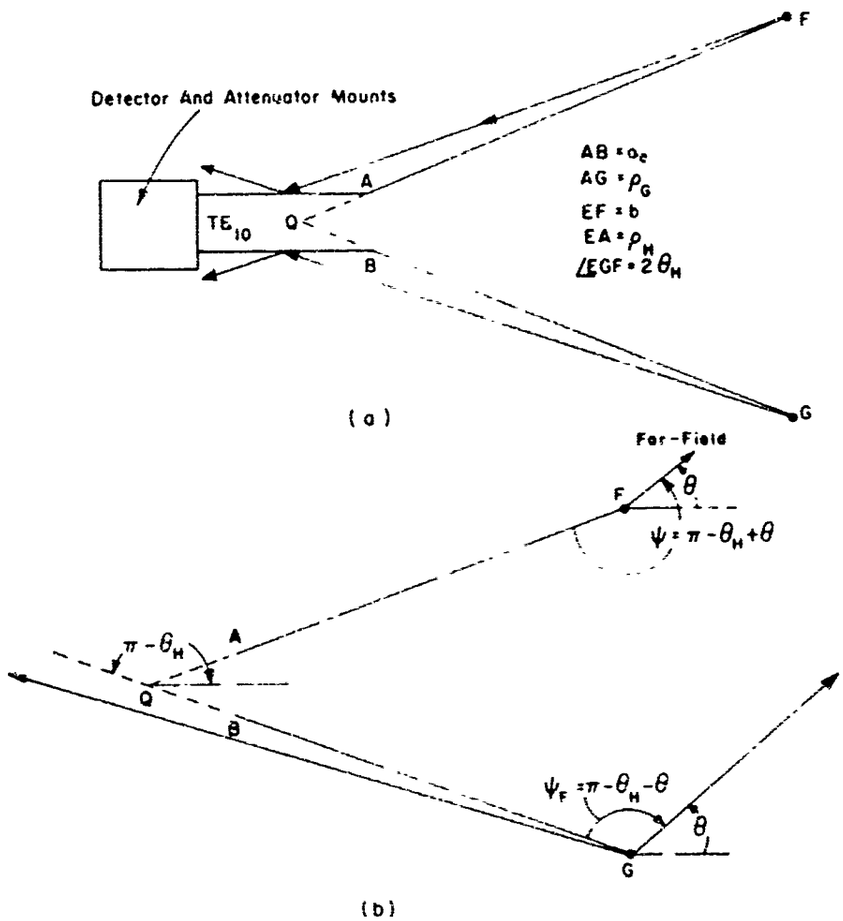

Fig. 7. Horn antenna (a) used in measurement and the Model (b) used in computation.

the diffracted ray from edge F and reflected by the guide surface shown in Fig. 7a is replaced by that directly diffracted from G. Using this approximate model, the total far-field pattern in the region $0 \leq \theta \leq \pi$ can be computed by Eq. (38) as

$$u_T(\theta) = u_H(\theta) + u_E(\theta), \qquad 0 \leq \theta \leq \pi,$$

where $u_H(\theta)$ is modified from Eq. (29) as

$$u_H(\theta) = D_A y_{FA} + D_B y_{FB} + (D_F)_T + (D_G)_T y_{FG} + \sum_{i=1}^{h} [I_{Li} y_{Fi} + I_{Ui} y_{FG} y_{Gi}] + \sum_{m=i}^{p-1} [I_{Lm} y_{Gm} y_{FG}],$$

(39)

$$\left.\begin{aligned} &D_A(\theta) : 0 \leq \theta \leq \theta_H \\ &D_B(\theta) : 0 \leq \theta \leq \theta_H + \psi_{oo} \end{aligned}\right\} \text{ Eqs. (10),}$$

$$\left.\begin{aligned} &D_F(\theta) : 0 \leq \theta \leq \pi \\ &D_G(\theta) : \begin{cases} 0 \leq \theta \leq \frac{\pi}{2} \\ -(\pi+\theta_H) \leq \theta \leq -\pi \end{cases} \end{aligned}\right\} \text{ Eqs. (22),}$$

$$\left.\begin{aligned} &I_{Li}(\theta) : 0 \leq \theta \leq \theta_H + \psi_{oi} \\ &I_{Ui}(\theta) : 0 \leq \theta \leq \theta_H - \psi_{oi} \end{aligned}\right\} \text{ Eqs. (16),}$$

$$I_{Lm}(\theta) : \frac{\pi}{2} - (m+1)\theta_H \leq \theta \leq \frac{\pi}{2} - m\theta_H, \quad \text{Eqs. (23),}$$

and $U_E(\theta)$ is modified from Eq. (35) as

(40) $$u_E(\theta) = u^*(o)[2\{D_1 y_{FD_1} + D_2 y_{FD_2}\}];$$

(40) (cont)

$$\left.\begin{array}{ll} D_1(\theta) & 0 \leq \theta \leq \theta_H \\ D_2(\theta) & \pi - \theta_H \leq \theta \leq \pi \end{array}\right\} \quad \text{Eqs. (34)} .$$

The phase-factors in Eqs. (39) and (40) can be obtained from Eqs. (28) and (37), respectively.

Computations of $u_H(\theta)$ and $u_E(\theta)$ are simple algebraic superpositions if the function v_B can be computed. The diffraction terms v_B of D_A, D_B, I_{Li}, and I_{Ui} are computed by making use of Eq. (A-11). The v_B of the rest of the terms in Eqs. (39) and (40) are computed by Eq. (A-10). The pattern computed for the parameters shown in Fig. 8 is plotted for

$$20 \log \frac{|u_T(\theta)|}{|u_T(0)|} .$$

For convenience of comparison, the computed pattern is shown displaced (+5) db above the measured pattern in Fig. 8. Excellent agreement is observed in the region $0 \leq \theta \leq 90°$. In the region $90° \leq \theta \leq 180° - \theta_H$, the radiation intensity is below (-50)db. Therefore, the experimental pattern cannot be accurately measured. In the backlobe region, $180° - \theta_H \leq \theta \leq 180°$, two computed patterns are shown. The dotted pattern is obtained by neglecting the contribution $U_E(\theta)$ from E-edges. The calculated pattern including $U_E(\theta)$ gives good agreement with the measured pattern.

V. CONCLUSIONS

Diffraction theory in conjunction with the method of images has been demonstrated to be a successful technique to compute the principal H-plane pattern of a horn antenna. The interactions between wedges A and B at the horn throat are successfully described by using a new form of diffraction function v_B. This new form of v_B is the series formulation in terms of cylindrical wave functions given in Eq. (A-9). The convergence of this series allows practical and accurate computation of v_B for typical horn antennas.

The contribution $U_E(\theta)$ from the E-edges has been shown to be the primary radiation in the backlobe region. In the main-lobe region, the

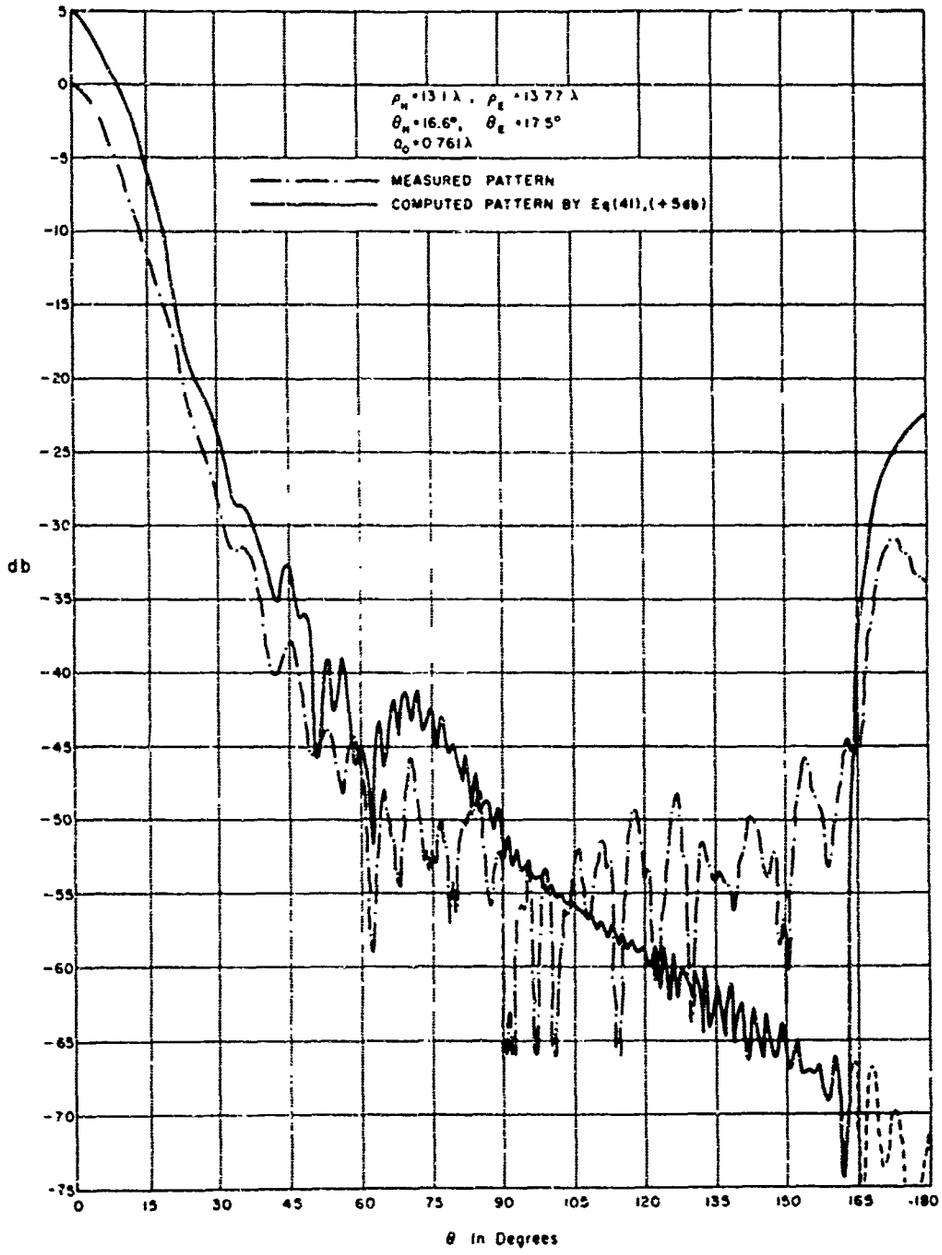

Fig. 8. Comparison of patterns.

contribution of $U_E(\theta)$ is unnoticiably small as compared to that of $u_H(\theta)$. The experimental results confirming the above conclusions have been given in Ref. 3.

A corrugated horn[6] of dimensions similar to those given in Fig. 8 has been discovered to have an E-plane pattern almost identical to that of H-plane in the figure. Therefore, by principles of duality, the discovery suggests that the E-plane pattern of a corrugated horn can be solved by treating the corrugated surfaces as magnetic conductors.

It may finally be concluded that the radiation mechanisms of horn antennas described by diffraction theory are new points of views on electromagnetic radiation and propagation. Proper use of the theory ensures solutions for most two-dimensional problems involving perfectly conducting wedges.

APPENDIX A
REVIEW OF DIFFRACTION THEORY

The two-dimensional problem of the electromagnetic field in the neighborhood of a conducting wedge illuminated by a uniform plane wave was first solved by Sommerfeld[9]. The solution for a conducting half-plane (zero wedge angle) was formulated in terms of the Fresnel integral. Subsequently, Pauli[10] formulated the solution for wedges of arbitrary angles in an asymptotic series in which the dominant term is the Fresnel integral. The higher-order terms in Pauli's solution become identically zero for zero wedge angle. Therefore, Pauli's solution is used here for the general case.

Figure A-1 shows the geometry of the wedge used by Pauli to formulate the solution of field intensity at $P(r, \psi)$ caused by plane-wave illumination. By reciprocity, if the same wedge of a perfectly conducting surface is illuminated by a uniform cylindrical wave from S shown in Fig. A-1b, the far-field intensity can be written from Pauli's solution as

$$v = v(\rho, \phi^+, n) \pm v(\rho, \phi^-, n), \tag{A-1}$$

$$= v^+ \pm v^-$$

$$\phi^\pm = \psi \mp \psi_o \text{ , and}$$

$$n = 2 - \frac{2\theta_o}{\pi} \text{ ,}$$

where the terms $v^\pm$ represent the incident and the reflected fields, respectively. The sum $(v^+ + v^-)$ applies when S is a magnetic line source, and the difference $(v^+ - v^-)$ applies if S is an electric line source. The incident and the reflected fields are composed of geometrical optics terms and diffracted terms, as,

$$v^\pm = (v^*)^\pm + v_B^\pm \text{ .}$$

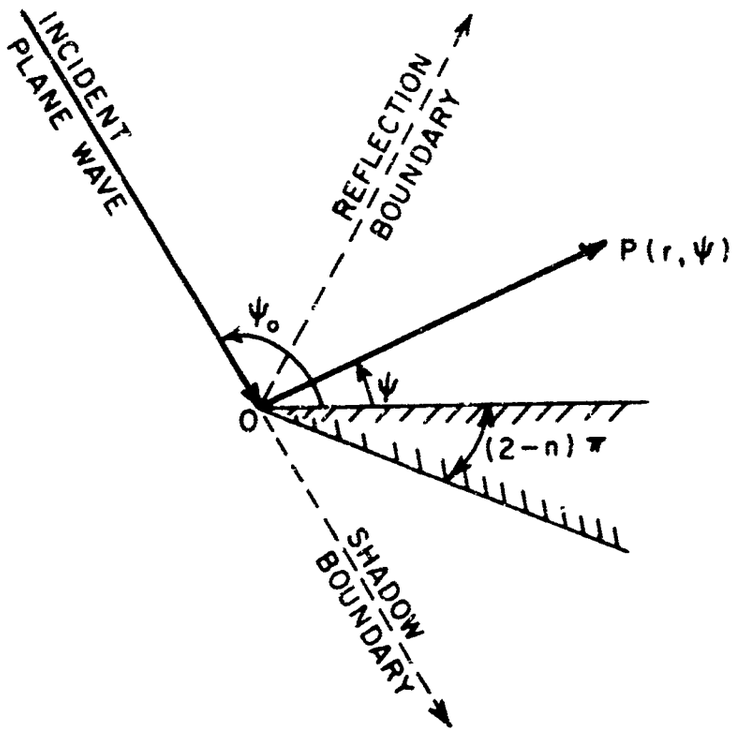

(a) Illuminated by a uniform plane wave

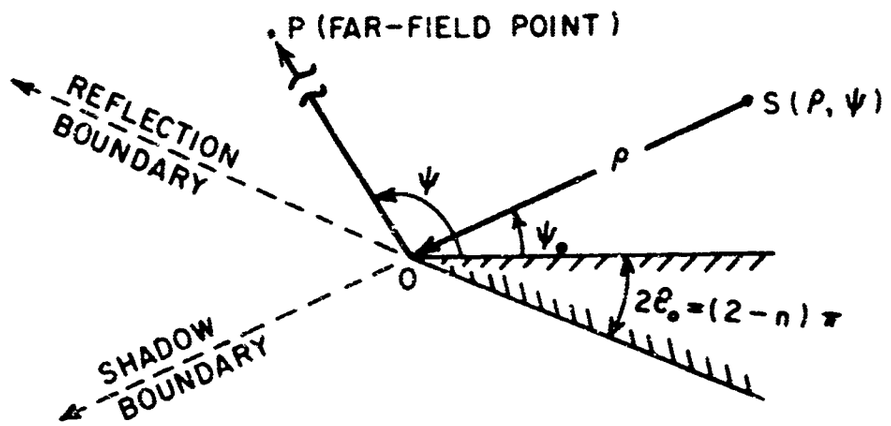

(b) Illuminated by uniform cylindrical wave

Fig. A-1. Geometry of a wedge.

The geometrical optics terms are given by

$$(A\text{-}2) \qquad (v^*)^{\pm} = v^*(\rho, \phi^{\pm}, n)$$

$$= \begin{cases} \mathrm{Exp}[jk\rho \cos(\phi^{\pm} + 2\pi nN)], & -\pi < \phi^{\pm} + 2\pi nN \leq \pi, \\ 0 & \text{otherwise} \end{cases}$$

$$N = 0, \pm 1, \pm 2 - - - ,$$

where the periodicity of the functions is seen to be $2n\pi$. The diffracted terms are given by

$$(A\text{-}3) \qquad v_B^{\pm} = v_B(\rho, \phi^{\pm}, n)$$

$$= \frac{\mathrm{Exp}(j\frac{\pi}{4})}{\sqrt{\pi}} \left(\sin\frac{\pi}{n}\right) \left[\frac{2\left|\cos\frac{\phi^{\pm}}{2}\right| \mathrm{Exp}\,(jk\rho\cos\phi^{\pm})}{\cos\frac{\pi}{n} - \cos\frac{\phi^{\pm}}{n}} \int_{\sqrt{ak\rho}}^{\infty} e^{-j\tau^2}\, d\tau \right.$$

$$\left. + \begin{pmatrix} \text{Higher-order terms} \\ \text{negligible for large } k\rho \end{pmatrix} \right]$$

and

$$a = 1 + \cos\phi^{\pm} .$$

As $(ak\rho)$ approaches infinity, i.e., as the line source S recedes to the infinity, the solutions in Eq. (32) can be written

$$(A\text{-}4) \qquad v_B(\rho, \phi^{\pm}, u) = \frac{\mathrm{Exp}\left[-j\left(\frac{\pi}{4} + k\rho\right)\right]}{\sqrt{2\pi k\rho}} \left[\frac{\sin\frac{\pi}{n}}{n\left(\cos\frac{\pi}{n} - \cos\frac{\phi^{\pm}}{n}\right)} \right] .$$

For N=0 in Eq. (A-2) the geometrical optics terms have discontinuities at the shadow boundary ($\phi^{+} = \pi$), and the reflection boundary ($\phi^{-} = \pi$). At these boundaries, the diffracted terms are given as

$$(A\text{-}5)\qquad v_B(\rho, \phi^{\pm}=\pi, n) = \begin{cases} -\frac{1}{2}\,\mathrm{Exp.}(-jk\rho) + \text{- - -} & \phi^{\pm} = \lim_{\epsilon \to 0}(\pi - \epsilon) \\ +\frac{1}{2}\,\mathrm{Exp.}(-jk\rho) + \text{- - -} & \phi^{\pm} = \lim_{\epsilon \to 0}(\pi + \epsilon) \end{cases},$$

where the higher-order terms are negligible for large $(k\rho)$ are not presented. The solutions are essential in ensuring continuity at the boundaries. Since we intentionally make the geometrical optics terms in Eq. (A-2) defined at the boundaries, $\phi^{\pm} = +\pi$, the first equation of Eq. (A-5) should be used to obtain the field intensities at the boundaries The total far-field of the wedge illuminated by a uniform cylindrical wave shown in Fig. A-1b can now be obtained by using Eqs. (A-2), (A-3), and (A-5) as

$$(A\text{-}6)\qquad u(\rho, \phi, n) = [(v^*)^+ + v_B{}^+] \pm [(v^*)^- + v_B{}^-] ,$$

where the reflection terms disappear if the wedge is illuminated by the source with $\psi_o = 0$. If the source is an electric line element, the value of $u(\rho, \phi, n)$ is identically zero for $\psi_o = 0$.

The solutions in Eq. (A-6) are valid only in evaluating the far-field intensity which is the main concern of present problem. The diffracted near-field intensities of a conducting half-plane, i.e., $n = 2$, have been solved by Nomura[11] and used by Ohba for dipole source illumination. Since this solution is in a general form, it can easily serve to illustrate principles of reciprocity. To generalize the solution further, the diffracted near-fields of a wedge illuminated by a line source have been written by Dybdal[12] in a form as follows:

$$(A\text{-}7)\qquad v(r, \rho, \phi^{\pm}, n) = \frac{\mathrm{Exp}\,[-jk(r+\rho-b)]}{\sqrt{r+\rho}}\,[v_B(b, \phi^{\pm}, n)]$$

$$b = \frac{r\rho}{r+\rho} ,$$

where the v_B terms are given in Eq. (A-3). If the field point is in the far-zone, $v(r, \rho, \phi^{\pm}, n)$ is reduced to

$$v(r, \rho, \phi^{\pm}, n) = \frac{\text{Exp}\,[-jkr]}{\sqrt{r}}\ [v_B(\rho, \phi^{\pm}, n)]\ ,$$

which, with the common factor $r^{-\frac{1}{2}}\,\text{Exp}[-jkr]$ removed, is identical to Eq. (A-3). If the source point recedes to the far-zone, the solutions in Eq. (A-7) are reduced to

$$v(r, \rho, \phi^{\pm}, n) = \frac{\text{Exp}[-jk\rho]}{\sqrt{\rho}}\ [v_B(r, \phi^{\pm}, n)]\ ,$$

which, with the common factor $\rho^{-\frac{1}{2}}\,\text{Exp}[-jk\rho]$ removed, are identical to the near-field solutions of a wedge illuminated by a uniform plane wave.

If a wedge has its value of n quite different from 2 and is illuminated by a line source located closer than several wavelengths from the wedge, the higher-order terms of $v_B(\rho, \phi^{\mp}, n)$ in Eq. (A-3) should be included to give accurate results. Instead of evaluating higher-order terms, a more convenient form of the solution for diffracted fields may be obtained from the series of cylindrical wave functions and can be written as

(A-8)
$$v_B(\rho, \phi^{\pm}, n) = v(\rho, \phi^{\pm}, n) - v^*(\rho, \phi^{\pm}, n),$$

$$v(\rho, \phi^{\pm}, n) = \frac{1}{n}\left[J_0(k\rho) + 2\sum_{m=1, 2, \ldots}^{\infty} (j)^{\frac{m}{n}} J_{\frac{m}{n}}(k\rho)\cos\frac{m}{n}(\phi^{\pm})\right],$$

and

$$v^*(\rho, \phi^{\pm}, n) = \begin{cases} \text{Exp}[jk\rho\cos(\phi^{\pm} \pm 2nN\pi)], \\ \qquad -\pi < \phi^{\pm} + 2nN\pi < \pi, \quad N = 0, \pm 1, \pm 2, \ldots. \\ 0, \qquad \text{otherwise}\ . \end{cases}$$

The quantities $v(\rho, \phi^{+}, n)$ and $v(\rho, \phi^{-}, n)$ are the incident and reflected terms of the total radiation field[13]. The geometrical-optics terms $v^*(\rho, \phi^{+}, n)$ and $v^*(\rho, \phi^{-}, n)$ are valid only in the defined regions and are set identically zero otherwise. Writing v_B explicitly as a function of ρ, ϕ, and n, we have

$$(A\text{-}9)\qquad v_B(\rho,\phi^{\pm},n)=\frac{1}{n}\left[J_o(k\rho)+2\sum_{m=1,2..}^{\infty}(j)^{\frac{m}{n}}J_{\frac{m}{n}}(k\rho)\cos\frac{m}{n}(\phi^{\pm})\right]$$

$$-\begin{cases}\mathrm{Exp}[jk\rho\cos(\phi^{\pm}+2nN\pi)], & -\pi<\phi^{\pm}+2nN\pi<\pi,\\ & N=0,\ \pm1,\ \pm2\ \ldots\text{-}\\ 0, \quad \text{otherwise.}\end{cases}$$

It is more convenient to use the Bessel function form to compute v_B when ρ is small, because in this case the Bessel functions converge rapidly. The angles $\phi^{\pm}$ in v_B may be replaced by $\phi^{i,r}$ to indicate more clearly that they are the field angles for incident and reflected terms, respectively. The diffraction terms $v_B(\rho,\phi,n)$ are calculated in two ways, depending on the values of ρ and n. For a wedge of zero wedge angle (n = 2) or for $\rho > 1.5\lambda$, the Fresnel integral form of v_B in Eq. (A-3) is used without the higher-order terms and is denoted by

$$(A\text{-}10)\qquad v_F(\rho,\phi^{\pm},n)=\frac{\mathrm{Exp}\left(j\frac{\pi}{4}\right)}{\sqrt{\pi}}\frac{\left(\sin\frac{\pi}{n}\right)}{n}\left[\frac{2\left|\cos\frac{\phi^{\pm}}{2}\right|\mathrm{Exp}(jk\rho\cos\phi^{\pm})}{\cos\frac{\pi}{n}-\cos\frac{\phi^{\pm}}{n}}\right.$$

$$\left.\int_{\sqrt{ak\rho}}^{\infty}e^{-j\tau^2}\,d\tau\right]$$

$$a=1+\cos\phi^{\pm}\ .$$

For cases in which $\rho < 1.5\lambda$ and $n \neq 2$, the series form of v_B in Eq. (A-9) involving Bessel functions is employed and is denoted by

$$(A\text{-}11)\qquad v_D(\rho,\phi^{\pm},n)=\frac{1}{n}\left[J_o(k\rho)+2\sum_{m=1,2..}^{15}(j)^{\frac{m}{n}}J_{\frac{m}{n}}(k\rho)\cos\frac{m}{n}(\phi^{\pm})\right]$$

$$-\begin{cases}\mathrm{Exp}[jk\rho\cos(\phi^{\pm}+2nN\pi)], & -\pi<\phi^{\pm}+2nN\pi<\pi\\ & N=0,\ \pm1,\ \pm2,\text{-----}\\ 0, \quad \text{otherwise,}\end{cases}$$

where the series is summed for $m/n \leq 15$ because the Bessel functions of order higher than 15 are vanishingly small[14] for $\rho \leq 1.5\lambda$.

APPENDIX B
FAR-FIELD WAVES FROM THE IMAGES OF LINE SOURCES

Consider line sources parallel to perfectly conducting plane walls. The problem in this Appendix is to obtain the far-field intensity of the image waves from the walls. The problem is a two-dimensional one and the line sources can be either magnetic or electric line sources.

First, a directional line source is shown at point S in Fig. B-1. If a semi-infinite conducting wall is placed with an angle θ_o with respect to the horizontal reference axis, the image of the line source is formed at point 1. The line source radiates a directional cylindrical wave to the

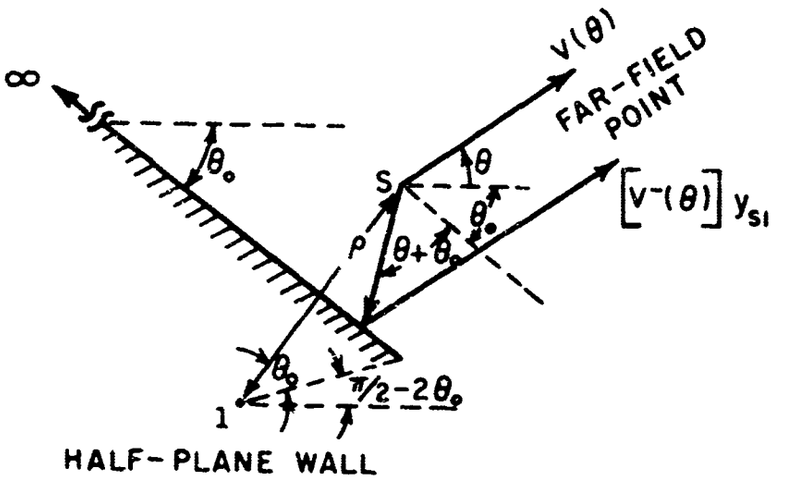

Fig. B-1. Geometry of a line source and its image.

far-field and it is designated as $v(\theta)$. In the presence of the wall, $v(\theta)$ is reflected by the wall in the region $-(\pi + \theta_o) \leq \theta \leq -\pi/2$. The reflected wave is called the image wave from point 1 and can be described by

$$(B\text{-}1) \qquad I_1(\theta) = v^-(\theta) = v(-2\theta_o - \theta), \qquad \frac{\pi}{2} - 2\theta_o \leq \theta \leq -(\pi - \theta_o),$$

where the superscript minus sign implies the reflection of $v(\theta)$. The total far-field pattern can then be obtained by superposition of the two waves as

(B-2) $$u(\theta) = v(\theta) \pm v(-2\theta_o - \theta)\, y_{s1}$$

and

$$y_{s1} = \mathrm{Exp}\left[-jk\rho \sin(\theta + \theta_o)\right] ,$$

where y_{s1} is the local phase-factor of the image referred to point S and ρ is the distance between the image and the source as shown in Fig. B-1. This result is obtained by removing the common factor $R^{-\frac{1}{2}} \mathrm{Exp}\left[-jkR\right]$, with R referred to S. The plus sign applies for a magnetic line source, while the minus sign should be used for an electric line source.

Next, a corner reflector of $2\theta_o$ is shown in Fig. B-2a. Let there be only one line source $v(\theta)$ at A. In the region $-(\pi - \theta_o) < \theta < -\pi/2$, the rays from A are reflected by the lower wall. Only rays in the ray -1 zone (from image -1) are directly reflected to the far-field. The rays in ray -2 zone are reflected twice while those in ray -3 zone are reflected three times inside the reflector. Consequently, three image waves are formed in three distinct regions. The first image wave can be written similar to Eq. (B-1) from Fig. B-2a as

(B-3) $$v_1^-(\theta) = v(-2\theta_o - \theta) , \qquad \frac{\pi}{2} - 2\theta_o \leq \theta \leq \frac{\pi}{2} - \theta_o ,$$

which is obtained by replacing the θ of $v(\theta)$ by $(-2\theta_o - \theta)$. The second image is formed in the upper wall. This image wave can be obtained by replacing the θ of $v_1^-(\theta)$ by $(+2\theta_o - \theta)$ as

(B-4) $$v_2^-(\theta) = v(-4\theta_o + \theta), \qquad -\left(\frac{\pi}{2} - 3\theta_o\right) \geq \theta \geq -\left(\frac{\pi}{2} - 2\theta_o\right) .$$

Again replacing the θ of the above expression by $(-2\theta_o - \theta)$, the third image wave can be obtained as

$$v_3^-(\theta) = v(-6\theta_o - \theta), \qquad \frac{\pi}{2} - 4\theta_o \leq \theta \leq \pi - 7\theta_o .$$

This process can be used for any number of images. The number of images is equal to the number of ray zones determined by the highest integer h such that $h < \pi/2\theta_o$. Construction of the images in Fig. B-2a can

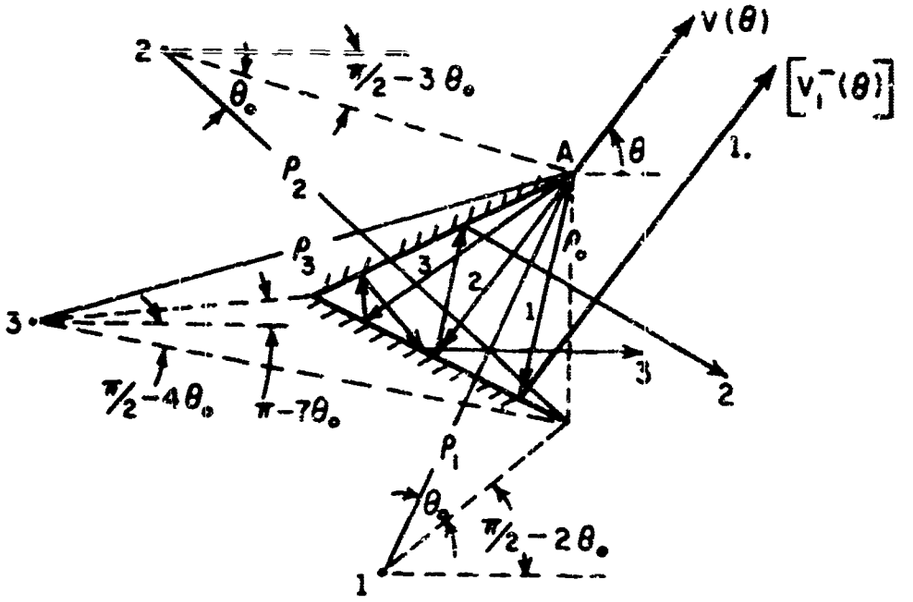

(a) Images due to a line source at A

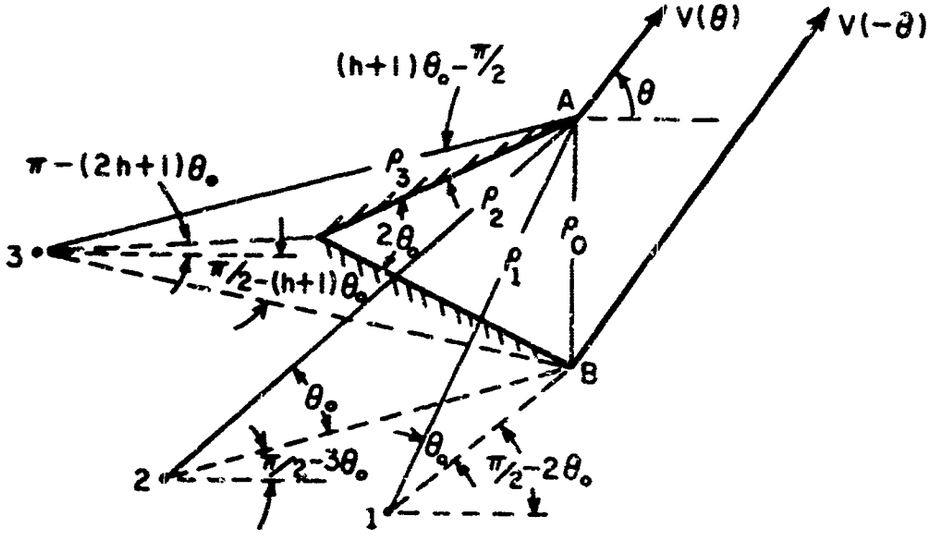

(b) Images of lower wall due to two symmetrical line sources

Fig. B-2. Geometry of a corner reflector $\frac{\pi}{3} > 2\theta_o > \frac{\pi}{4}$.

be extended to conclude that all the odd-numbered images are formed in the lower wall, while the even-numbered images are in the upper wall. In general, the image waves can be written

$$(B\text{-}5) \qquad v_i^-(\theta) = \begin{cases} v(-2i\theta_o - \theta), & \frac{\pi}{2} - (i+1)\theta_o \leq \theta \leq \frac{\pi}{2} - i\theta_o \qquad \text{for i odd} \\ v(-2i\theta_o + \theta), & -\left[\frac{\pi}{2} - (i+1)\theta_o\right] \geq \theta \geq -\left[\frac{\pi}{2} - i\theta_o\right] \text{ for i even,} \end{cases}$$

$$i = 1, 2, 3 - -- (h-1) .$$

If the ratio of π to $2\theta_o$ is not exactly an integer, the valid region of the last image should be modified as

$$(B\text{-}6) \qquad v_h^-(\theta) = \begin{cases} v(-2h\theta_o - \theta), & \frac{\pi}{2} - (h+1)\theta_o \leq \theta \leq \pi - (2h+1)\theta_o \qquad h \text{ odd} \\ v(-2h\theta_o + \theta), & -\left[\frac{\pi}{2} - (h+1)\theta_o\right] \geq \theta \geq -\left[\pi - (2h+1)\theta_o\right] \; h \text{ even} . \end{cases}$$

The value of $2\theta_o$ in Fig. B-2 is larger than $\pi/4$ but smaller than $\pi/2$. Therefore h is equal to 3 and the last image is defined by Eq. (B-6) for h odd.

Figure B-2b shows two symmetrical line sources at A and B from which far-field waves $v(\theta)$ and $v(-\theta)$, respectively, are radiated. The images of the source at A are identical to those in Fig. B-2. Because of the symmetrical properties of the assumed line sources and the geometry of the reflector, the images resulting from the source at B are symmetrical to those of A. Consequently, equal numbers of symmetrical images are formed in both walls of the reflector. Making use of this symmetry, the image waves excited by $v(-\theta)$ from B can be obtained similar to Eq. (B-5) as

$$(B\text{-}7) \qquad v_i^-(-\theta) = \begin{cases} v(-2i\theta_o + \theta), & -\left[\frac{\pi}{2} - (i+1)\theta_o\right] \geq \theta \geq -\left[\frac{\pi}{2} - i\theta_o\right] \qquad \text{i odd} \\ v(-2i\theta_o - \theta), & \frac{\pi}{2} - (i+1)\theta_o \leq \theta \leq \frac{\pi}{2} - i\theta_o \qquad \text{i even,} \end{cases}$$

$$i = 1, 2, 3 --- (h-1) .$$

In case the ratio π to $2\theta_o$ is not an integer, the last image wave has its defined region as in Eq. (B-6) by interchanging h odd and h even.

Comparison of Eqs. (B-5) to (B-7) indicates that all image waves from the lower wall are combinations of $v_i^-(\theta)$ with i odd and $v_i^-(-\theta)$ with i even. The other set of combinations gives the image waves from the upper wall. To summarize, the image waves from both walls of the reflector are designated by $(I_L)_i$ and $(I_U)_i$ as follows:

(B-8) $$(I_L)_i = v^-(\theta) = v(-2i\theta_o - \theta) \quad , \quad \frac{\pi}{2} - (i+1)\theta_o \leq \theta \leq \frac{\pi}{2} - i\theta_o, \qquad \text{lower wall;}$$

$$(I_U)_i = v^-(-\theta) = v(-2i\theta_o + \theta) \quad , \quad -\left[\frac{\pi}{2} - (i+1)\theta_o\right] \geq \theta \geq -\left[\frac{\pi}{2} - i\theta_o\right], \text{ upper wall;}$$

$$i = 1, 2, 3, \text{---} \; h \; .$$

For the ratio of π to $2\theta_o$ not an integer, modifications for i = h are

(B-9) $$(I_L)_h = v(-2h\theta_o - \theta), \quad \frac{\pi}{2} - (h+1)\theta_o \leq \theta \leq \pi - (2h+1)\theta_o;$$

and

$$(I_U)_h = v(-2h\theta_o + \theta), \quad -\left[\frac{\pi}{2} - (h+1)\theta_o\right] \geq \theta \geq -\left[\pi - (2h+1)\theta_o\right] \; .$$

In Fig. B-2b, three images in the lower wall are shown. Their far-field intensities can be obtained by setting h = 3 in Eqs. (B-8) and (B-9).

Because of symmetry, only the upper-half region $0 \leq \theta \leq \pi$ needs to be considered for the radiation pattern of the reflector antenna. In this region, the contributions are from the sources at A and B and the images in the lower wall. Contributions from the last image in the upper wall are possible, if the ratio of π to $2\theta_o$ is not an integer. Superposition of all these contributions gives the total far-field $u(\theta)$ as

(B-10) $$u(\theta) = v(\theta) + [v(-\theta)]y_{AB} + \sum_{i=1}^{h} (\pm 1)^i \, [v(-2i\theta_o - \theta)]y_{Ai}$$

$$+ (\pm 1)^h \, [v(-2h\theta_o + \theta)]y_{AB} \, y_{Bh} \; ,$$

where $(+1)^i$ preceding the image terms are used for magnetic line sources and $(-1)^i$ are used for electric line sources. The phase factors are introduced by taking A as phase-reference:

(B-11)
$$y_{AB} = \text{Exp}\,[-jk\rho_o \sin\theta],$$

$$y_{Ai} = \text{Exp}\,[-jk\rho_i \sin(i\theta_o+\theta)],$$

$$y_{Bh} = \text{Exp}\,[-jk\rho_h \sin(h\theta_o-\theta)],$$

$$\rho_o = AB, \text{ and}$$

$$\rho_i = \rho_{i-1}\cos\theta_o + \rho_o \cos(i\theta_o).$$

The above expressions can be obtained by considering the geometry of Fig. B-2. It is noted that each term in Eqs. (B-10) and (B-11) is set zero outside its defined region.

REFERENCES

1. Yu, J.S. and Rudduck, R.C., "The E-Plane Pattern of An Antenna Model for Horn Antennas," Report 1767-3, 1 April 1965, Antenna Laboratory, The Ohio State University Research Foundation. This report is in process.

2. Ye, B., Kinber, "Diffraction at the Open End of a Sectoral Horn," Radio Engn. and Electronic Physics, 7-10, 1620-1622, (Oct., 1962).

3. "Final Engineering Report," Report 1423-7, 1 November 1963, Antenna Laboratory, The Ohio State University Research Foundation; prepared under Contract Number AF 30(602)-2711, Rome Air Development Center, Griffiss Air Force Base, N. Y. (RADC-TDR-63-549) (AD 600 652).

4. Ohba, Y., "On the Radiation Pattern of a Corner Reflector Finite in Width," IEEE Trans. on Antennas and Propagations, AP-11:2, 127-132, (March 1963).

5. Terman, F.E., Electronic and Radio Engineering, McGraw-Hill Book Company, Inc., New York (1955), pp. 140-143.

6. Ryan, C.E. Jr., and Rudduck, R.C., "Calculation of the Radiation Pattern of a General Parallel-Plate Waveguide Aperture for the TEM and TE_{01} Waveguide Modes," Report 1693-4, 10 September 1964, The Antenna Laboratory, The Ohio State University Research Foundation; prepared under Contract Number N62269-2184, U.S. Naval Air Development Center, Johnsville, Pennsylvania.

7. Keller, J.B., "Geometrical Theory of Diffraction," J. Opt. Soc. Am., 52-2, 116-130, (February, 1962).

8. Lawrie, R.E., Peters, L. Jr., and Davis, C.H., "Modification of Horn Antennas for Low Side Level," Report 1767-2, March, 1965, Antenna Laboratory, The Ohio State University Research Foundation; prepared under Contract Number AF 30(602)-3269, Rome Air Development Center, Griffiss Air Force Base, N. Y.

9. Sommerfeld, A., Optics, Academic Press, Inc., New York (1954), pp. 245-265.

10. Pauli, W., "On Asymptotic Series for Functions in the Theory of Diffraction of Light," Phys. Rev., 54, 924-931, (December, 1938).

11. Nomura, Y., "On the Diffraction of Electromagnetic Waves by a Perfectly Reflecting Wedge," Scientific Reports, B-1 and 2, No. 1, Res. Inst. Tohoku University, Japan, (1951), pp. 1-24.

12. Dybdal, R. B., "Mutual Coupling Between TEM and TE_{01} Parallel-Plate Waveguide Apertures," Report 1693-[illegible], 15 August 1964, Antenna Laboratory, The Ohio State University Research Foundation; prepared under Contract Number N62269-2184, U. S. Naval Air Development Center, Johnsville, Penna.

13. Harrington, R. F., Time-Harmonic Electromagnetic Fields, McGraw-Hill Book Company, Inc., New York (1961), pp. 238-242.

14. Jahnke, E. and Emde, F., Tables of Functions, Dover Publications, New York (1945), p. 174.